Available online at www.sciencedirect.com
SCIENCE DIRECT®
Journal of Catalysis 223 (2004) 44–53
JOURNAL OF CATALYSIS
www.elsevier.com/locate/jcat

Inelastic neutron scattering investigation on the site occupation of atomic hydrogen on platinum particles of different size

Peter W. Albers,[a,*] Marco Lopez,[b] Gerhard Sextl,[b] Gerald Jeske,[c] and Stewart F. Parker[d]

[a] *Degussa AG, Wolfgang Industrial Site, Department of Physical Chemistry, Rodenbacher Chaussee 4, D-63457 Hanau (Wolfgang), Germany*
[b] *Umicore AG&Co KG, Fuel Cells, Rodenbacher Chaussee 4, D-63403 Hanau (Wolfgang), Germany*
[c] *Umicore AG&Co KG, Precious Metal Chemistry, Rodenbacher Chaussee 4, D-63403 Hanau (Wolfgang), Germany*
[d] *ISIS Facility, Rutherford Appleton Laboratory, Chilton, Didcot, Oxfordshire, OX11 0QX, UK*

Received 8 October 2003; revised 17 December 2003; accepted 23 December 2003

Abstract

The site occupation of atomic hydrogen in the topmost atomic layers of fuel cell catalysts was studied. Platinum and platinum/ruthenium particles of varying dispersity supported on carbon black and unsupported particles of platinum black were investigated by means of inelastic neutron scattering. The materials were hydrogenated inside of in situ neutron cells and were measured under frozen hydrogen sorption equilibrium. Transmission electron microscopy revealed the stability of the dispersion of the supported precious metals to the alternating in situ hydrogenation/dehydrogenation cycles. With increasing particle size the vibrational mode of atomic hydrogen on nanodisperse platinum in the range of 500–600 cm^{-1} was narrowed and its maximum signal shifted down to lower energies. The H occupation of (111) terraces of the platinum particles increased. The relative intensities of the INS scattering contributions from C_{4v} sites at about 460 and 650 cm^{-1} decreased. The most prominent spectral changes were observed in the transition region around 3.0–4.8 nm of the average primary particle size of the precious metal which according to Kinoshita (J. Electrochem. Soc. 137 (1990) 845) is correlated to specific electrocatalytic activity. It was possible to discriminate between the vibrational modes of hydrogen atoms on different surface sites on platinum, Pt–OH groups, Pt_x/Ru_y–OH groups, and traces of water. The Pt–OH translational modes ranged from 200 to 400 cm^{-1}. The Pt–OH bending modes were observed at 840, 950, and 1016 cm^{-1} for platinum black and at 810, 877, and 954 cm^{-1} for supported Pt/Ru particles exhibiting also Pt_2Ru and $PtRu_2$ sites. Water and Pt–OH groups are formed during the first interactions between gaseous hydrogen and the catalyst surface. The extraction of residual traces of oxygen from larger precious metal particles by hydrogen cycling procedures seemed to be limited by diffusion phenomena. This was of minor relevance for nanodisperse platinum species.

Keywords: Fuel cell catalysts; Precious metal dispersion; Hydrogen; Atomic hydrogen; Hydroxyl groups; Site occupation; Pt (111); Pt(100); Nanoparticles; Platinum; Ruthenium; Platinum black; Carbon black; Inelastic incoherent neutron scattering; Transmission electron microscopy

1. Introduction

In situ characterization and detailed investigation of the surface states of atomic hydrogen in the topmost atomic layers of platinum-based catalysts at hydrogen loadings which are relevant for the technical applications is of high importance for a better understanding of the activity and selectivity in many catalytic systems. Supported platinum catalysts are used (e.g.) in catalytic hydrogenations of aromatic molecules such as nitroaromatic compounds to anilines, the conversion of imines to amines, in reductive amination or alkylations, and many other processes [1–3]. Prominent applications of supported or unsupported platinum or of platinum alloys of different shapes and dispersity are gas/solid reactions such as the BMA process (synthesis of HCN from CH_4 and NH_3) [4], the oxidation of ammonia in the production of nitric acid [5], automotive exhaust gas purification systems [6–9], and, to a steadily growing extent, the use in fuel cell catalysts [10–12]. Especially in fuel cell catalysis very finely divided platinum particles are used on adequate support materials such as special grades of carbon black. Techniques for investigating the interactions between platinum particles and protons under realistic conditions are of paramount interest in fundamental research on platinum catalysts as well as the economic aspects of catalyst development and

* Corresponding author.
E-mail address: peter.albers@degussa.com (P.W. Albers).

0021-9517/$ – see front matter
doi:10.1016/j.jcat.2003.12.018

detailed optimization of the catalysts morphology and performance. Unfortunately, due to the physical properties of (e.g.) Pt/C or Pt,Ru/C catalysts which are used in fuel cell applications (high dispersity of the carbon black support, tailored nanodispersity of the precious metal components, electrical conductivity of the support materials, high absorption of electromagnetic radiation inside of the catalyst), the use of techniques such as nuclear magnetic resonance or infrared and Raman techniques is very complicated.

In previous work it was shown that inelastic incoherent neutron scattering (IINS or INS) is uniquely suitable for identifing and discriminating between the states of atomic and of molecular hydrogen species at the surfaces of highly dispersed platinum catalysts under realistic hydrogen pressures [13,14]. Therefore, INS appears to be an attractive and relevant tool for investigations on fuel cell catalysts and, more commonly, for studying catalytic hydrogenations.

For the case of Pt on carbon supports in electrocatalytical applications Ross and co-workers concluded [15,16] that (111) and (110) faces are less effective for oxygen reduction than the (100) crystal face. Kinoshita [12] reported a correlation between the fraction of Pt surface atoms on the (100) and (111) crystal faces of the Pt particles of cubooctahedral structures, with varying particle size and the specific catalytic activity of Pt electrocatalysts (Fig. 3 in Ref. [12]).

For cubooctahedral particles—which in addition to (111) faces also show (100) sites—an optimum in mass activity at 3.5 nm Pt particle diameter was reported. Under these conditions the surface fraction of Pt on (100) and (111) faces shows a maximum according to changes of the coordination number with changing average particle size. Details on the statistics of surface atoms and surface sites on metal catalysts were given in the work of Van Hardeveld and Hartog [17,18] (for cubooctahedral particles see (e.g.) Figs. 10 and 18 in Ref. [17]).

In the present study we have addressed these points by comparing the interactions between hydrogen and nanodisperse platinum and platinum/ruthenium particles on carbon black supports at different particle sizes. Furthermore, for the purpose of comparison, the hydrogen/platinum interactions in the case of unsupported platinum black particles were monitored. It was, indeed, expected that the INS technique might also give some direct evidence of changes of the site occupation of atomic hydrogen species in the topmost atomic layers of platinum particles under the conditions of varying precious metal dispersion as well as with the atomic dispersion—e.g., in the case of supported Pt/Ru particles which are used in the anode catalyst of fuel cells. This should also be of some future relevance for many other applications of finely divided platinum particles in heterogeneous catalysis.

The in situ INS measurements were supported by results from transmission electron microscopy.

Table 1
Sample numbers and composition of the supported and unsupported platinum catalysts

Sample No.	Composition (wt%)
1	40% Pt/C
2	40% Pt/C
3	40% Pt/C
4	(40% Pt + 20% Ru)/C
5	Platinum black

2. Experimental

2.1. Pt/C, Pt,Ru/C catalysts, and Pt black

Since the focus of the present study was to reveal the site occupation of atomic hydrogen on platinum particles of different size, laboratory samples were prepared and selected according to the particle-size evaluations by means of TEM on fresh electrocatalysts.

Different 40% Pt/C (wt%) catalysts and a 40% Pt/20% Ru/C (wt%) catalyst were prepared according to the usual wet-impregnation procedure well documented in the literature (see, e.g., [19–21]). The sample identification is given in Table 1. The same preparation procedure was used on the samples whose INS spectra were reported in [14]. The hydrogen content of the carbon black support was determined by means of a LECO-RH-404 hydrogen analyzer as 2030 (±200) ppm.

High surface area platinum black (purity 99.98%, BET surface area 35 m^2/g, Umicore) was measured as a reference for the characteristics of unsupported Pt particles. The average particle sizes of the aggregates and the agglomerates of the unsupported platinum were in the range of about 70 nm (TEM). These structures were formed by primary particles of smaller size (about 10–30 nm). The Pt lattice parameter was 0.3923 nm (determined by X-ray diffraction, XRD).

2.2. Neutron spectroscopy (INS)

The electrocatalysts and the platinum blacks were sealed into thin-walled aluminum (99.99%) cells which were evacuated to 10^{-5} mbar using a turbomolecular pump (Leybold) and a double-stage rotary pump with a zeolite-type adsorption trap to prevent backdiffusion of traces of moisture or contamination with aliphatic material. The cells were sealed by means of welded bellow valves (Nupro).

Afterward, in the case of the supported platinum catalysts, a sample was slowly exposed to hydrogen (99.999% Messer-Griesheim) at 22 °C in steps of a few millibars each over several days using a gas volumetric device including capacitive pressure transducers (MKS Baratron). The adsorption was controlled such that a pronounced macroscopic heating of the catalyst powder due to the heat of adsorption was avoided during the H_2/Pt interactions. In the first step, the equilibrium pressure of hydrogen in a sample can was limited to 100 mbar. Afterward the can was pumped

out again ending with the vacuum of the turbomolecular pump. The procedure was repeated in a second hydrogenation cycle ending with 300 mbar. Afterward the hydrogenation/dehydrogenation cycle was repeated three times ending with 1.5 bar each. This procedure was chosen to carefully remove residual amounts of oxygen, water, and volatile organic species from the catalysts surface and to activate and to accommodate the surface for controlled hydrogen uptake. The adsorption activity of the catalysts to hydrogen was monitored by gas volumetric methods. After removal of the hydrogen in a final step the cans were loaded to the final equilibrium pressures noted in the figures and sealed in the aluminum cans prior to the in situ INS experiment.

The INS spectra were measured on a TOSCA spectrometer at the ISIS pulsed neutron facility (Rutherford Appleton Laboratory, UK) [22,23]. Before and during the experiments the samples were cooled down to 20 K using a closed-cycle helium cryostat. Therefore, residual traces of water as shown in the spectrum in Fig. 12 are condensed to ice.

The beam size was 4 cm × 4 cm. This allowed macroscopic amounts of sample (about 40 g of catalyst) to be characterized at a bulk level by one single spectrum. However, a consequence of the large amount of catalyst which is necessary to obtain adequate spectra of the hydride species is a distinct background contribution which must be removed from the spectra.

After an INS measurement the hydrogen was removed from a can by 24 h of evacuation with a turbomolecular pump. During this procedure, after at least 12 h of pumping, a can was heated for 3 h up to 200 °C using a specially designed furnace that fitted tightly to the Al cells. Afterward background spectra of the dehydrogenated supported Pt/C and Pt,Ru/C catalysts were recorded and subtracted, respectively. This procedure was finally chosen after several series of experiments on these catalysts because it was observed that a rather complete decomposition of the hydrides inside the cans could be achieved only after enhanced times of pumping and heating. Furthermore, partial changes of small proportions of the carbonaceous supports could be induced by the hydrogen cycling procedure and spillover phenomena. Therefore, the background subtractions in the figures partly appear as incomplete due to these influences. However, they were the best to be obtained for the given experiments as a compromise between careful hydrogenation/dehydrogenation for retaining the given precious metal dispersion on the one hand and for removing traces of water and, sufficiently, decomposing the hydride species in the sample can on the other.

The spectra were normalized to the actual sample weight. Nevertheless, a comparison of absolute scattering intensities is beyond the scope of the discussion in Section 3.2.

The platinum black was treated under similar conditions. However, due to the fact that pronounced particle growth of the unsupported (!) platinum black particles may occur even under moderate hydrogenation/dehydrogenation cycles loss of BET surface area by sintering could not be completely avoided according to the exothermal hydrogen/platinum interactions inside the sample can. Furthermore, residual oxygen species which are converted into water molecules during the first periods of interaction with hydrogen had to be removed before an adequately pure platinum hydride surface could be established (see Section 3.2, Figs. 11A–C).

Contary to palladium black which even at a hydrogen equilibrium pressure of a few millibars contains a dominant proportion of protons in bulk states (screened protons on octahedral sites [24,25]) the protons of platinum hydride are predominantly located in surface regions [26]. Therefore, surface species dominate the INS spectra in Figs. 11A–C. This requires a dedicated optimization of hydrogenation/dehydrogenation conditions until a clean surface hydride is obtained and signal contributions of water species can be excluded. Therefore, in the case of sample 5 the evacuation times were enhanced up to several days each and the speed of hydrogen dosing was rather low: starting from high vacuum conditions a hydrogen-loading/-deloading cycle from 1 mbar H_2 up to 1 bar H_2 and back to high vacuum was realized in the time scale of 5 days. Nevertheless, starting with a BET surface area of 35 m^2/g the hydrogenation/dehydrogenation cycles on the platinum black led to a lower surface area due to more or less pronounced sintering of the unsupported particles. The final nitrogen surface area of the black was 18 m^2/g. After recording the in situ INS spectrum of sample 5 the platinum hydride was decomposed by evacuating the can with a turbomolecular pump for 12 h and by degassing the sample for 3 h at 200 °C in vacuo. Immediately after cooling down, the background spectrum of the dehydrogenated platinum black sample was recorded. Inspection of Fig 11B shows that there is still some residual hydrogen (peak at about 500 cm^{-1}) present on the Pt black even after prolonged dehydrogenation. To obtain a subtraction that contained information on all the sites occupied, this was artificially removed by drawing a straight line between 420 and 570 cm^{-1}.

2.3. Transmission electron microscopy (TEM)

After performing the in situ INS investigations the cans with the finally dehydrogenated but still pyrophoric catalyst samples (Section 2.2) were carefully flushed with argon gas (99.995%) and then were slowly opened under streaming argon. A specimen of a catalyst was prepared on holey carbon foil supported by a copper grid (400 mesh) and immediately afterward was transferred into an analytical Jeol 2010-F transmission electron microscope. For digital imaging a CCD camera was utilized (GATAN 794). The microscope was operated at 200 keV primary beam energy. Energy dispersive X-ray analyses (EDX, Noran Voyager 4) were performed to probe the homogeneity of the 40%/20% Pt/Ru catalyst down to the nanoscale level.

TEM images as shown in Section 3.1 were taken to compare the size, shape, and distribution of the precious metal particles obtained after the hydrogenation/dehydrogenation

Table 2
Average precious metal particle (PM) size as determined by means of transmission electron microscopy before (be) and after (af) the neutron experiments

Sample No.	PM particle size, TEM (be) (nm)	PM particle size, TEM (af) (nm)
1	2.8	3.0
2	3.4	3.7
3	4.5	4.8
4	7.8	8.2

treatments. The average particle size (Table 2) was determined by statistical evaluations of the TEM micrographs.

3. Results and discussion

3.1. Transmission electron microscopy

A set of typical TEM images of the samples 1, 3, and 4 is presented in Figs. 1–6. They illustrate that after conditioning of the catalysts by in situ hydrogenation and dehydrogenation cycles and, finally, after degassing at 200 °C inside of the INS cells, an adequate lateral distribution of the precious metal particles at the surface of the carbon black support is retained.

Figs. 1–3 show images taken at lower magnification. They demonstrate the good dispersion, adhesion, and interaction between the precious metal particles and the carbon black support. Figs. 4–6 were taken at high magnification. The turbostratic arrangement of the graphite-like platelets of the basic structural units in the spherical geometry of the paracrystalline carbon black support can be clearly discriminated from the crystalline structure of the supported precious metal particles.

The average particle sizes as determined by statistical evaluations of about 500 supported precious metal particles in numerous TEM micrographs are given in Table 2. Comparison with the work of Kinoshita on the interdependencies among catalytic mass activity, crystallite size of the platinum particle, and the mass fraction of (100) and (111) surface atoms (shown in Fig. 3 in Ref. [12]) indicates that the average particle sizes of the catalyst sample Nos. 1–4 are suitable to cover a representative range around the maximum of catalytic activity and its decrease with increasing particle size. The trend of an increase of the particle size for sample $1 < 3 < 4$ is clearly illustrated by Figs. 1–6.

For the case of the Pt/Ru catalyst (Figs. 3 and 6) it was verified by numerous EDX spot analyses that the expected stoichiometry of 50 at% Pt/50 at% Ru was also established at the nanoscale level. No discrete Pt or Ru entities were observable. It follows that pure Pt_3 or Ru_3 surface sites are of minor or no importance. Either Pt_2Ru or $PtRu_2$ should be anticipated. The lattice spacings (d values) of pure, isolated entities of Ru or ruthenium oxides [27,28] could not be observed.

Since, at least in principle, the precious metal surface which is effective in the hydrogen/solid interactions is highest with the lowest particle size it can be expected that the relative contributions of hydrogen on coarse particles to the neutron spectra presented in the following section are much lower than that of the hydrogen on the nanodisperse precious metal particles with sizes in the range of about 3–8 nm (Table 2). The INS spectra in Section 3.2 should, therefore, be goverened by hydrogenous scattering of atomic hydrogen on the nanodisperse precious metal particles which clearly dominate (by number) samples 1–3 and also sample 4 (Table 2). Lattice imaging of the precious metal particles in the high-resolution mode (Figs. 4–6) revealed d spacings of about 0.23–0.22 nm. From X-ray diffraction [29–31] on platinum 0.2265 nm is known for hkl (111) (JCPDS 04-0802).

Figs. 7–9 were taken from a coarse particle of the platinum black (sample 5). These particles are of granular structure—aggregates and agglomerates which are formed by primary particles. These primary entities are strongly linked together during precipitation of the black and due to the subsequent particle growth during the in situ hydrogenation/dehydrogenation procedures in the INS cell. At higher resolution (Figs. 8 and 9) the crystallinity of the basic structural units of these aggregates is revealed. The different orientations of primary crystallites in Fig. 9 show d spacings of 0.23–0.22 and 0.19–0.20 nm according to the (111) and the (200) orientation (reference X-ray diffraction: 0.2265 and 0.1962 nm [29–31]).

3.2. Inelastic neutron scattering

Fig. 10 shows the difference spectra of the hydrogenated and the dehydrogenated supported electrocatalysts with 40% of Pt loading. The equilibrium pressure values which were established inside of the sample cans before the in situ INS experiments are noted in the captions. According to TEM (Table 2) the electrocatalyst No. 1 (Fig. 10A) showed the finest precious metal particles (Table 2). Distinct variations of, and differences between, the fine features of the bands at about 400–800 and 800–1200 cm^{-1} with increasing particle size are readily seen (Figs. 10B, C, D). All these spectra are dominated by the hydrogenous scattering of atomic hydrogen species on finely divided supported platinum (A–C) and of supported platinum/ruthenium particles (D) of increasing size. For the following discussion we refer to the detailed assignments of these signals of hydrogen on platinum in different sites as given in [13,14,32, and literature cited therein].

The signals at about 470 and 550 cm^{-1} are assigned to the E modes of the fourfold and threefold sites, respectively. The signal at about 650 cm^{-1} is assigned to the bending mode of the on-top species and the *A1* mode of the fourfold site.

Figs. 10A–D, suggest that with increasing primary particle size of the supported precious metals the major spectral contribution at around 500–600 cm^{-1} is narrowed and its signal maximum shifts down to lower energies (Ta-

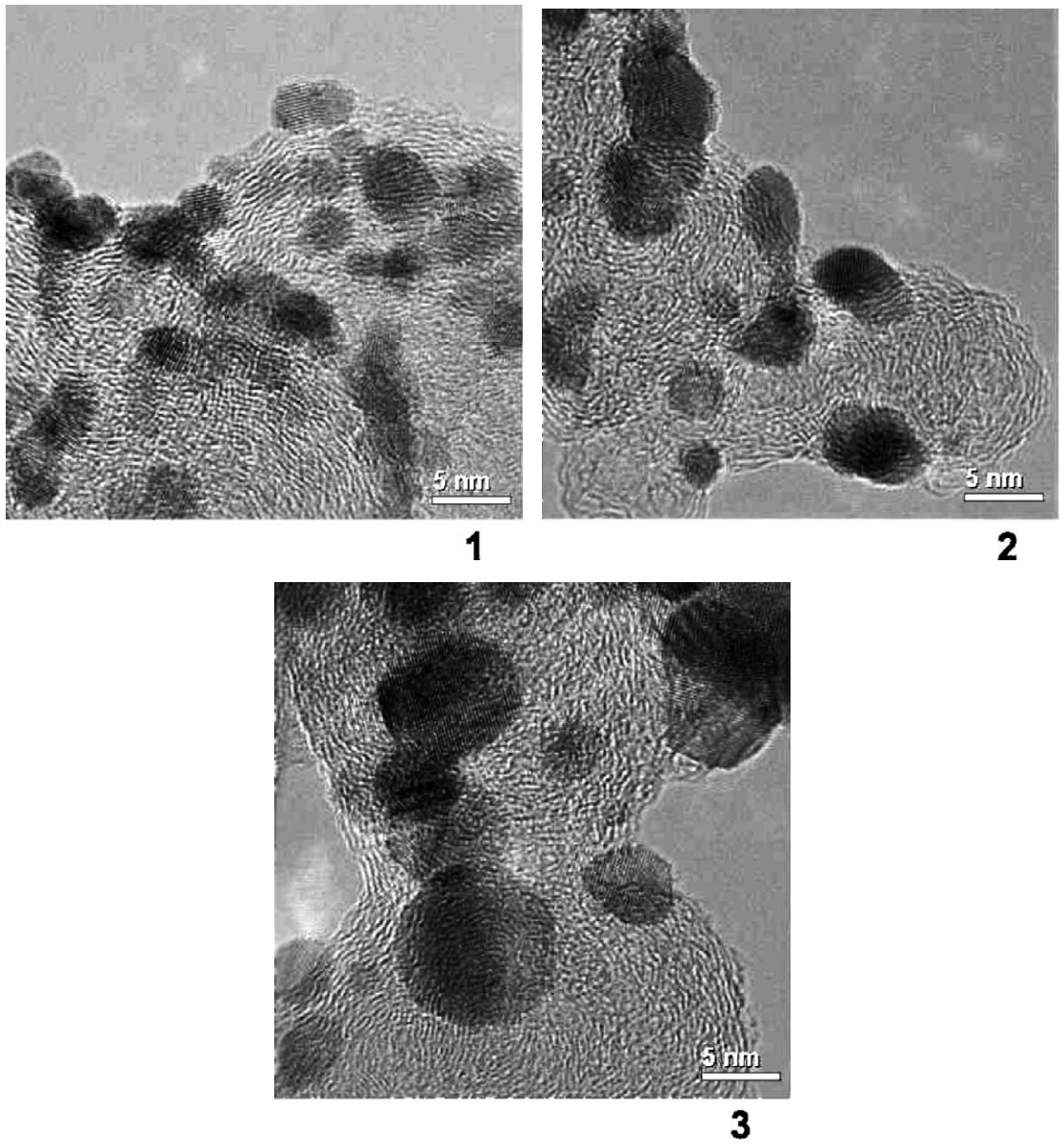

Figs. 1–3. Enhanced electron optical magnification ×200,000. (1 and 2) 40% platinum on carbon black, samples 1 and 3. (3) 40% of platinum/20% of ruthenium on carbon black, sample 4. STEM/EDX revealed that Pt and Ru are atomically dispersed and mixed at the nanoscale level.

ble 3): sample 1, 564 cm^{-1}; sample 2, 553 cm^{-1}; sample 3, 537 cm^{-1}; sample 4, 530 cm^{-1}. This trend continues with the unsupported platinum hydride shown in Fig. 11C: the signal is shifted down to 515 cm^{-1}.

With increasing size of the platinum particles the relative amount of (111) terraces increases. The atomic hydrogen on C_{3v} sites increasingly dominates the spectra of the supported 4.8 and 8.2 nm precious metal particles and is at the highest level in the spectrum of the comparatively coarse unsupported platinum black particles. The relative contributions from C_{4v} sites at about 460 and 650 cm^{-1} decrease (Figs. 10A–D, Fig. 11C, Table 4) and the signal region is narrowed at both sides of the dominating C_{3v} signal. This result is in qualitative agreement with the conclusions of Kinoshita on the optimum in mass activity at 3.5 nm precious metal particle size: the fraction of H surface species in (100) and (111) crystal faces changes significantly between samples 1–5. The most prominent changes in terms of signal narrowing and loss of C_{4v} site occupation are observed in the transition region of the precious metal particles size between about 3.0 and 4.8 nm (Figs. 10A–C).

We conclude that with increasing size of the precious metal particles the relative amount of (111) planes increases and the strength of interaction between the predominant sites and the atomic hydrogen entities changes. It is lowered as indicated by the signal shift from 564 cm^{-1} down to 515 cm^{-1} (Table 3).

Comparison of the spectra of the finely dispersed (Figs. 10A–C) and of the larger precious metal particles (Fig. 10D and Fig. 11) shows that additional and more or less

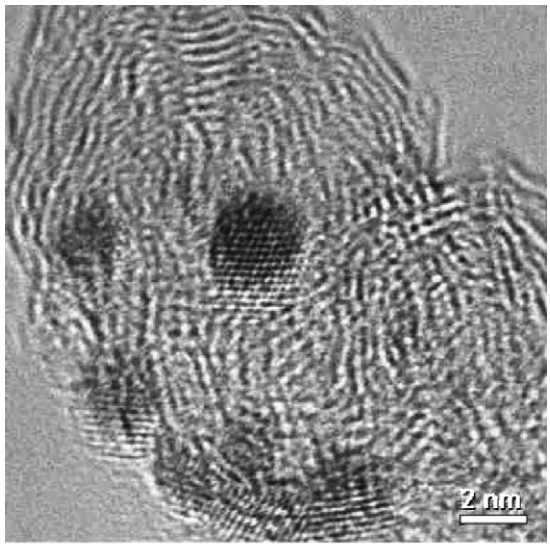

4

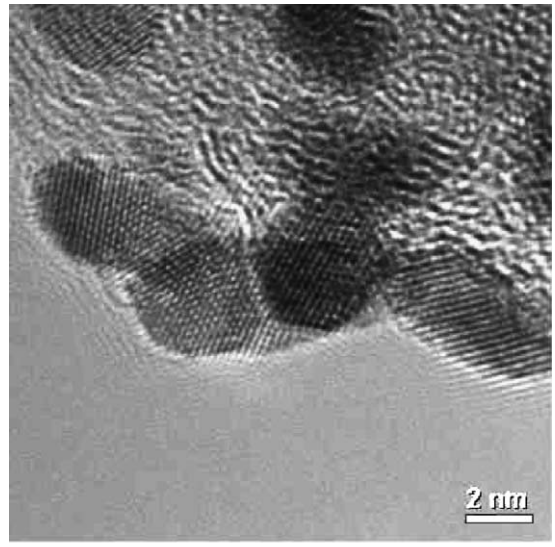

5

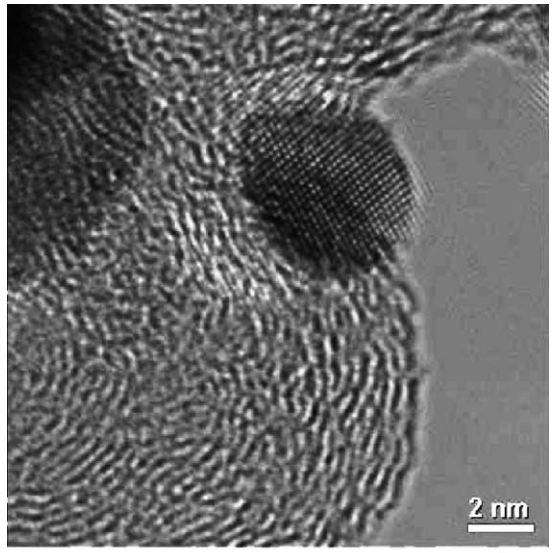

6

Figs. 4–6. Same as Figs. 1–3. High-resolution work; electron optical magnification ×1,000,000. (4 and 5) 40% platinum on carbon black, samples 1 and 3. (6) 40% of platinum/20% of ruthenium on carbon black, sample 4.

sharp bands are observed in the latter cases. Since these additional signals are rather sharp, hydrogen-containing species at the particle surface are also expected to be involved. With respect to interactions between residual oxygen at the catalyst surface and the hydrogen inside the INS sample cans the presence of Pt–OH groups may be anticipated. Regarding the results from recent work of Ertl and co-workers [33,34] on the vibrational states of H on Pt (111) and on OH on Pt (111) together with neutron data on H on supported Pt catalysts [13,14], the following assignments can be made: the sharp peak in Fig. 11C at 515 cm^{-1} is also due to hydrogen on platinum, preferably in C_{3v} sites. The other peaks at 200–400 cm^{-1} are due to Pt–OH translational modes. The signals at about 840, 950, and 1016 are Pt–OH bending modes with different degrees of hydrogen bonding [34]. The 1400 cm^{-1} signal appears as too strong to be correlated with Pt–H. The overtone of the Pt–H is probably buried under the Pt–OH bending bands at 800–1200 cm^{-1}. It can be understood that the 1400 cm^{-1} signal is a combination band of the Pt–OH frustrated translational modes at 200–400 cm^{-1} and the stretch/bend modes at 850–1250 cm^{-1}.

The Pt–OH bending modes of sample 4 appear at 810, 877, and 954 cm^{-1} (Fig. 10D) which according to TEM shows a homogeneous elemental distribution at the atomic scale. These frequencies are lower than the values measured for the pure platinum black sample 5. Since sample 4 contains finely dispersed Pt/Ru particles, the OH vibrations on Pt_2Ru or $PtRu_2$ sites must considered. At an average particle size of 8.2 nm (TEM) enhanced contributions of C_{3v} sites should be present. Regarding the 1:1 Pt:Ru stoichiometry it

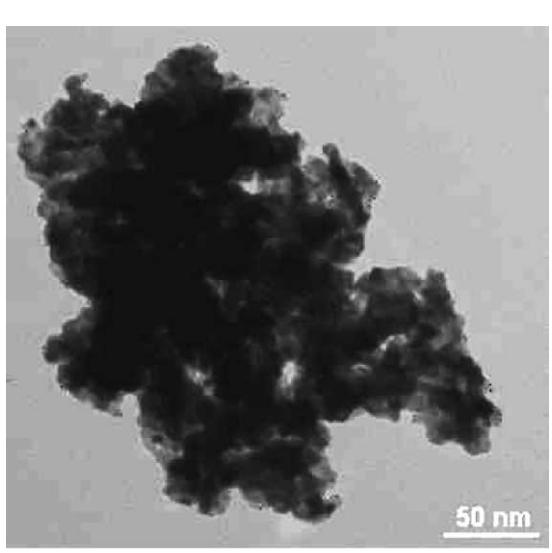

7

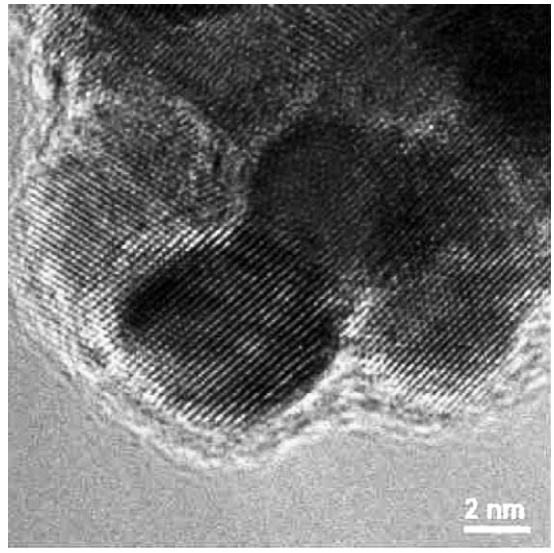

8

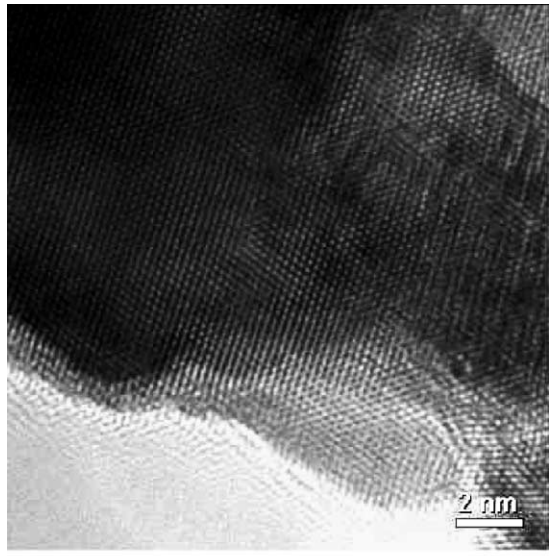

9

Figs. 7–9. (7) Survey image of platinum black, sample 5; electron optical magnification ×400,000. (8 and 9) High-resolution work; electron optical magnification ×1,000,000.

appears that there are no pure Pt_3 or Ru_3 surface sites. Either Pt_2Ru or $PtRu_2$ sites are anticipated. Therefore, the INS spectrum of the Pt/Ru/C sample is dominated by hydrogen on platinum in C_{3v} sites and by the sharp signals of metal–OH vibrations in surface sites formed by Pt and Ru atoms.

Regarding the HREELS data for H on Ru single crystal surfaces which were published by Christmann et al. [35,36] and related work [37–42] a strong preference for threefold sites of the Ru surface seems most likely. Vibrational modes at about 847 and 1146 cm^{-1} (//modes) and at 1210 cm^{-1} (perpendicular mode) are expected. Signal contributions at these energies cannot be unambiguously derived from Fig. 10D: no additional Ru/H signals as reported for pure Ru crystals were observed for the supported Pt/Ru species. Again, it follows that the INS spectrum 10D is dominated by Pt/H and Pt_x/Ru_y–OH vibrations. For investigations on interactions between hydrogen and pure supported ruthenium additional INS work is required as started by Mitchell et al. [43].

Fig. 12 shows the INS spectrum of catalyst 4 which was recorded after insufficient, short-term preconditioning in the in situ cell. The sample was treated in the fresh state by only two cycles of slow hydrogenation and dehydrogenation, ending with 300 mbar of equilibrium pressure in the INS cell. The neutron spectrum is dominated by the vibrational modes of water. Very similar results were obtained for the platinum black after short-term preconditioning. Since the INS spectra were recorded at 20 K, residual traces of, predominantly, reaction water as formed by converting residual oxygen from the surface or the near surface regions of the catalyst under

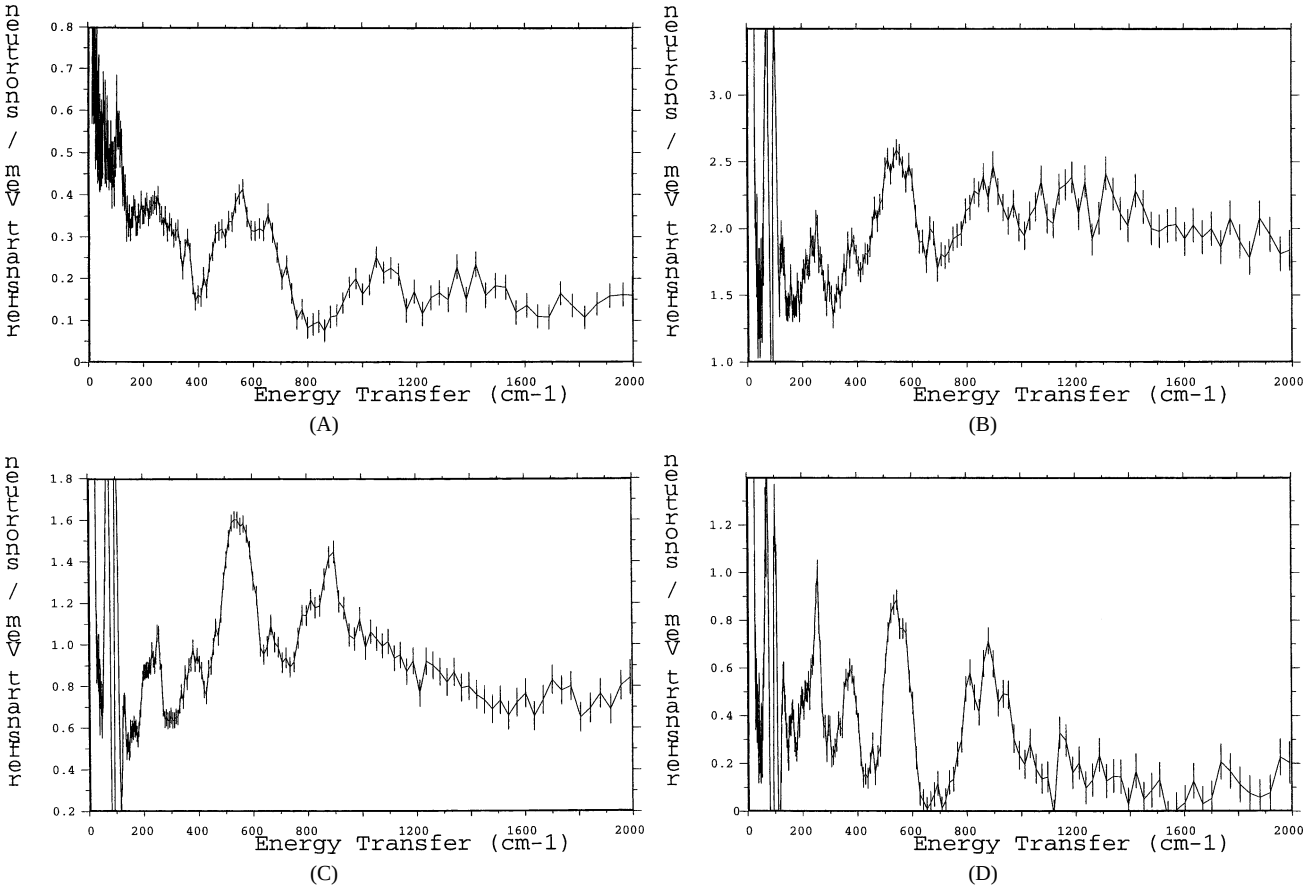

Fig. 10. INS spectra. Proton dynamics of supported precious metal particles on carbon black. A–D are difference spectra: INS spectrum of platinum catalysts as measured under in situ conditions under hydrogen equilibrium pressure minus the corresponding INS spectrum of a catalyst after pumping off the hydrogen at 200 °C. (n.b.: the average primary particle size increases from A to D.) (A) 40% Pt/C (800 mbar H_2 equilibrium pressure), sample 1. (B) 40% Pt/C (1000 mbar H_2 equilibrium pressure), sample 2. (C) 40% Pt/C (1000 mbar H_2 equilibrium pressure), sample 3. (D) 40% Pt/20% Ru/C (1000 mbar H_2 equilibrium pressure), sample 4.

Table 3
Signal positions of the Pt/H vibrations and signal assignments (please see text)

Sample	cm^{-1}	cm^{-1}	cm^{-1}
1	467	564	653
2	466	553	673
3	462	537	661
4	(455)	530	(?)
5	(?)	515	(?) (650)
Assignments	C_{4v} (*E*)	C_{3v} (*E*)	C_{4v} (*A1*) and On-top bending

the access of hydrogen are condensed into ice. From detailed INS work on the different phases of ice in the pure state [44,45] or supported species of ice on and in various carbons [46,47] the position of the leading edge of the intermolecular vibrational modes of this condensed water in the ice-like state is well known. The broad cliff-like feature at about 600–1100 cm^{-1} can be assigned to ice of Ih or Ic classification [44] due to water molecules which are condensed in unrestricted geometry at the surface of the catalyst particles. The intermolecular translational vibration of the condensed water molecules appears at about 50 cm^{-1}. From Fig. 12 it is evident that during the first cycles of moderate hydrogen treatment (Section 2.2) water was formed at the surface of the catalyst which could not be removed completely during the pumping procedure. It was formed at the catalyst surface by hydrogenous extraction of residual oxygen species. The amount of water present on the surface was determined by assuming that it was present as ice 1 h and comparing the integrated intensity of the water librational modes with a spectrum of a known quantity of ice. The error in the measurement is on the order of 10%. These approximate evaluations gave the result that at least about two monolayers of water were adsorbed at the surface of the material. The strong hydrogenous scattering contribution of these traces dominates the INS spectrum.

This observation confirms our previous interpretations: the additional bands of Pt–OH and Pt_x/Ru_y–OH groups in the spectra of the larger unsupported and the supported platinum particles (Fig. 11C and Fig. 10D) which are missing or of minor importance for the highly dispersed platinum species (Figs. 10A–C) can be traced back to residual species of oxygen at the surfaces of the catalysts (Pt–O, Pt–OH, Ru–O species, etc.) and, potentially, also to residual traces

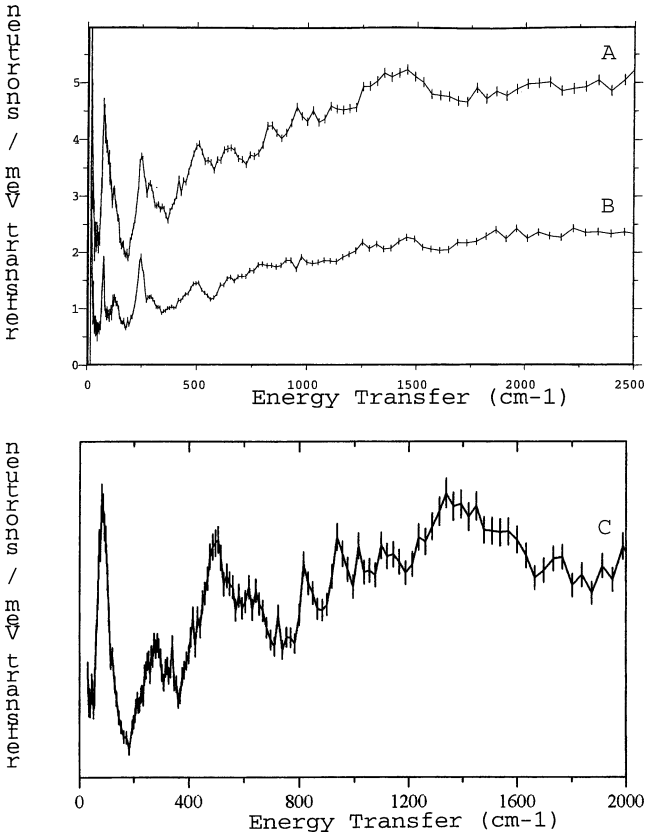

Fig. 11. (A) INS spectrum of platinum black recorded under 53 mbar of hydrogen, sample 5. (B) As A after dehydrogenation (background spectrum). (C) Difference spectrum A–B.

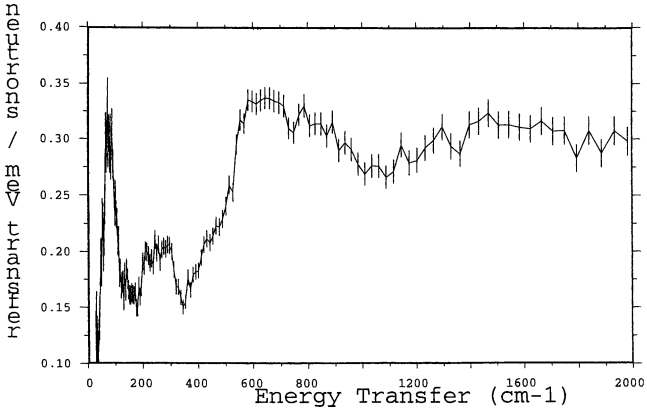

Fig. 12. INS spectrum of catalyst 4 after short-term hydrogenation. The spectrum is dominated by condensed water species which were formed during the first interactions between traces of residual oxygen from the surface and the hydrogen.

of oxygen in the selvedge or the bulk of the coarse platinum particles. Diffusion to the surface under the access of hydrogen occurs. The oxygen species are extracted and converted under the influence of hydrogen during the subsequent cycles of in situ hydrogenations/dehydrogenations. Water and Pt–OH or Pt_xRu_y–OH groups are formed, respectively. After removing the water molecules by extended pumping times at room temperature and by hydrogen cycling (Section 2 and Figs. 10 and 11) hydroxyl groups are found at the surface of the coarser platinum particles (Figs. 11 and 10D). A delay in the process of releasing and extracting the residual traces of oxygen is of minor relevance for the nanodisperse supported platinum particles. These conclusions seem in line with recent density functional calculations on the water production reaction on Pt(111) by Karlberg et al. [48].

An alternative or additional explanation would be a higher stability of hydroxyl groups on (111) planes with rather dense Pt–Pt coordination compared to the more open structure of (100) planes [17,18].

This finding may be of some relevance with respect to the relative amounts of reaction water and hydroxyl groups formed during the first steps of hydrogenation or preconditioning of platinum catalysts of varying dispersity in catalyst activation and catalyst formation procedures. Extended induction periods and varying adsorption properties may be of some concern in practical applications.

Finally, a comparison of Figs. 10–12 clearly confirms that the hydrogenous scattering in Figs. 10A–D and 11 is not dominated by the vibrational modes of water molecules: platinum/hydrogen species and –OH groups are measured, undisturbed by adventitious signal overlap with the hydrogenous scattering contributions of strongly adsorbed, condensed water molecules in the ice-like state.

4. Conclusions

In situ INS is uniquely suitable for revealing the site occupation of atomic hydrogen in the topmost atomic regions of fuel cell catalysts. The identification of certain surface species on nanodisperse platinum and platinum/ruthenium particles supported on high conductivity and highly absorbing carbon black and also of platinum black is possible.

With increasing particle size the vibrational mode of hydrogen on platinum at 500–600 cm^{-1} is narrowed and its maximum signal shifts down to lower energies. The occupation of (111) terraces increases. INS scattering contributions from C4v sites at about 460 and 650 cm^{-1} decrease. The most prominent spectral changes were observed in the transition region around 3.0–4.8 nm of precious metal particle size which according to Kinoshita is correlated to changes of the specific electrocatalytical activity.

INS made it possible to discriminate directly between the vibrational modes of hydrogen atoms on different surface sites on platinum, Pt–OH groups, Pt_x/Ru_y–OH groups and traces of adsorbed water. The Pt–OH translational modes ranged from 200 to 400 cm^{-1}. The Pt–OH bending modes were observed at 840, 950, and 1016 cm^{-1} for platinum black and at 810, 877, and 954 cm^{-1} for supported highly dispersed Pt/Ru particles, exhibiting Pt_2Ru and $PtRu_2$ sites. Water, Pt–OH and Pt_x/Ru_y–OH groups are formed during the first interactions between the gaseous hydrogen and the catalyst surface. The extraction of traces of oxygen from the

material by in situ hydrogen cycling procedures seems to be limited by diffusion phenomena as observed for coarse Pt particles. The stability of the –OH groups may be higher on (111) than on (100) planes.

An excellent stability of the precious metal dispersion to alternating hydrogenation/dehydrogenation cycles in the neutron cell was observed.

Acknowledgments

We thank the CLRC and the Rutherford Appleton Laboratory (UK) for access to the ISIS neutron facility. John Bones (ISIS) is thanked for the construction of the special furnace for the aftertreatments of the in situ sample cans. Robert Schwarz (Umicore) is gratefully acknowledged for the catalyst preparation and Winfried Weber (Degussa, Wolfgang Industrial Site) for the TEM investigations. Cedomir Gegic, Alberto Müller, Heribert Trageser, and colleagues (Degussa, Wolfgang Industrial Site) are thanked for the skilful preparation of the Al-sample holders for the in situ work.

References

[1] P. Rylander, Catalytic Hydrogenation in Organic Synthesis, Academic Press, New York, 1979.
[2] E. Auer, A. Freund, J. Pietsch, T. Tacke, Appl. Catal. A 173 (1998) 259.
[3] A.G. Degussa (Ed.), Edelmetall-Taschenbuch, Hüthig, Heidelberg, 2002, pp. 351–400.
[4] H. Klenk, A. Griffiths, K. Huthmacher, H. Itzel, H. Knorre, C. Voigt, O. Weiberg, in: W. Gerhartz, Y. Yamamoto, F.T. Campbell, R. Pfefferkorn, J.F. Rounsaville (Eds.), Ullmann's Encyclopedia of Industrial Chemistry, vol. A8, fifth ed., VCH, Weinheim, 1987, pp. 159–163.
[5] M. Thiemann, E. Scheibler, K.W. Wiegand, in: W. Gerhartz, Y. Yamamoto, F.T. Campbell, R. Pfefferkorn, J.F. Rounsaville (Eds.), Ullmann's Encyclopedia of Industrial Chemistry, vol. A17, fifth ed., VCH, Weinheim, 1987, pp. 293–339.
[6] K.C. Taylor, in: J.R. Anderson, M. Boudart (Eds.), Catalysis-Science and Technology, Springer, Berlin, 1984, p. 140.
[7] E.S.J. Lox, B.H. Engler, in: G. Ertl, H. Knözinger, J. Weitkamp (Eds.), Handbook of Heterogeneous Catalysis, vol. 4, VCH, Weinheim, 1997.
[8] E.S.J. Lox, B.H. Engler, E. Koberstein, in: A. Crucq (Ed.), Catalysis and Automotive Pollution Control II, Elsevier, Amsterdam, 1991, p. 291.
[9] T. Kreuzer, E.S. Lox, D. Lindner, J. Leyrer, Catal. Today 29 (1996) 17.
[10] W.R. Grove, Philos. Mag. 14 (1839) 127.
[11] G.J. Acres, J.C. Frost, G.A. Hards, R.J. Potter, T.R. Ralph, D. Thompsett, G.T. Burstein, G.J. Hutchings, Catal. Today 38 (1997) 393.
[12] K. Kinoshita, J. Electrochem. Soc. 137 (1990) 845.
[13] A.J. Renouprez, H. Jobic, J. Catal. 113 (1988) 509, and literature cited therein.
[14] P. Albers, E. Auer, K. Ruth, S.F. Parker, J. Catal. 196 (2000) 174, and literature cited therein.
[15] M.L. Sattler, P.N. Ross, Ultramicroscopy 20 (1986) 21.
[16] P.N. Ross, J. Electrochem. Soc. 126 (1979) 78.
[17] R. Van Hardeveld, F. Hartog, Surf. Sci. 15 (1969) 189.
[18] R. Van Hardeveld, F. Hartog, in: D.D. Eley, H. Pines, P.B. Weisz (Eds.), Advances in Catalysis, Academic Press, New York, 1972, p. 75.
[19] M. Che, O. Clause, C. Marcilly, in: G. Ertl, H. Knözinger, J. Weitkamp (Eds.), Handbook of Heterogeneous Catalysis, vol. 1, VCH, Weinheim, 1997.
[20] N. Giordano, E. Passalacqua, L. Pino, A.S. Arico, K. Antonucci, M. Vivaldi, K. Kinoshita, Electrochim. Acta 36 (1991) 1979.
[21] A. Honji, T. Mori, Y. Hishinuma, J. Electrochem. Soc. 137 (1990) 2084.
[22] Z.A. Bowden, M. Celli, F. Cilloco, D. Colognesi, R.J. Newport, S.F. Parker, F.P. Ricci, V. Rossi-Albertini, F. Sacchetti, J. Tomkinson, M. Zoppi, Phys. B 276–278 (2000) 98.
[23] D. Colognesi, M. Celli, E. Cilloco, R.J. Newport, S.F. Parker, V. Rossi-Albertini, E. Sacchetti, J. Tomkinson, M. Zoppi, Appl. Phys. A 74 (2002) 564;
S.F. Parker, J. Neutron Res. 10 (2002) 173.
[24] F.A. Lewis, The Palladium Hydrogen System, Academic Press, London, 1967.
[25] E. Wicke, H. Brodowski, in: G. Alefeld, J. Völkl (Eds.), Hydrogen in Metals II, in: Topics in Appl. Phys., vol. 29, Springer, Berlin, 1978, p. 73.
[26] E. Raub, in: E. Fromm, E. Gebhardt, (Eds.), Gase und Kohlenstoff in Metallen, Springer, Berlin, p. 648, and literature cited therein.
[27] JCPDS 06-0663 Ru metal: hexagonal a, 2.7058; c, 4.2819; d value 0.2056 nm.
[28] JCPDS 40-1290 RuO_2: tetragonal a, 4.4994; c, 3.1071; d value 0.3183 nm.
[29] N.V. Ageev, V.G. Kuznetsov, Izvest. Akad. Nauk SSSR (Khim) (1937) 753–755.
[30] M. Hansen, K. Anderko, in: Constitution of Binary Alloys, McGraw–Hill, New York, 1958, p. 1138.
[31] JCPDS 04-0802 Pt metal: cubic a, 3.9231; d value 0.2265 nm.
[32] P. Albers, S.F. Parker, ISIS annual report, Rutherford Appleton Laboratory, CLRC, Oxon, UK 2001 (RB No. 12031).
[33] S.C. Badescu, P. Salo, T. Ala-Nissila, S.C. Ying, K. Jacobi, Y. Wang, K. Bedürftig, G. Ertl, Phys. Rev. Lett. 88 (2002) 136101.
[34] K. Bedürftig, S. Völkening, Y. Wang, J. Wintterlin, K. Jacobi, G. Ertl, J. Chem. Phys. 111 (1999) 11147.
[35] G. Lauth, E. Schwarz, K. Christmann, J. Chem. Phys. 91 (1989) 3729.
[36] K. Christmann, G. Lauth, E. Schwarz, Vacuum 41 (1990) 293.
[37] M. Gruyters, K. Jacobi, J. Electron. Spectrosc. Relat. Phenom. 64/65 (1993) 591.
[38] C.Y. Fan, K. Jacobi, Surf. Sci. 313 (2001) 21.
[39] M.A. Barteau, J.Q. Broughton, D. Menzel, Surf. Sci. 133 (1983) 443.
[40] H. Shi, K. Jacobi, Surf. Sci. 313 (1994) 289.
[41] H. Feibelmann, D.R. Hamann, Surf. Sci. 179 (1987) 153.
[42] M.Y. Chou, J.R. Chelikowsky, Phys. Rev. B 39 (1989) 5623.
[43] P.C.H. Mitchell, S.F. Parker, J. Tomkinson, D. Thompsett, J. Chem. Soc., Faraday Trans. 95 (1998) 1489.
[44] I. Kolesnikov, J.-C. Li, S.F. Parker, R.S. Eccleston, C.-K. Loog, Phys. Rev. 59 (1999) 3569.
[45] J.-C. Li, J.D. London, D.K. Ross, J.L. Finney, J. Tomkinson, W.F. Sherman, J. Chem. Phys. 94 (1991) 6770.
[46] P. Albers, A. Karl, J. Mathias, D.K. Ross, S.F. Parker, Carbon 39 (2001) 1663.
[47] P. Albers, K. Seibold, G. Prescher, B. Freund, S.F. Parker, J. Tomkinson, Carbon 37 (1999) 437.
[48] G.S. Karlberg, F.E. Olsson, M. Persson, G. Wahnström, J. Chem. Phys. 119 (2003) 4865.